Desalination and Water Treatment
www.deswater.com

doi: 10.5004/dwt.2023.29804

304 (2023) 140–149
August

Boron-containing compounds as a new candidate for supercapacitor electrode: simplified synthesis and structural identification properties

Murat Akdemir[a], Hilal Demir Kivrak[b], Ahmet Kilic[c], Levent Beyazsakal[c], Mustafa Kaya[d,b], Sabit Horoz[e,*]

[a]*Department of Electrical and Electronics Engineering, Faculty of Engineering, Siirt University, Siirt 56100, Turkey, email: muratakdemir@siirt.edu.tr*
[b]*Department of Chemical Engineering, Faculty of Engineering and Architecture, Eskisehir Osmangazi University, Eskişehir 26040, Turkey, email: hilaldemir.kivrak@ogu.edu.tr*
[c]*Department of Chemistry, Faculty of Art and Science, Harran University, Sanliurfa 63190, Turkey, email: leventbeyazsakal@gmail.com (L. Beyazsakal)*
[d]*Department of Chemical Engineering, Faculty of Engineering, Siirt University, Siirt 56100, Turkey, email: mustafakaya@siirt.edu.tr*
[e]*Department of Metallurgical and Materials Engineering, Faculty of Natural Sciences and Engineering, Sivas Science and Technology University, 58100 Sivas, Turkey, email: sabit.horoz@sivas.edu.tr*

Received 14 October 2022; Accepted 22 July 2023

ABSTRACT

In this study, the performance of two boron-containing compounds, $C_{14}H_{14}BNO_2{\cdot}HCl$ (BCC_1) and $C_{38}H_{38}B_2Cl_2N_4O_4$ (BCC_2), as electrodes in supercapacitor applications was investigated in the presence of Na_2SO_4 and KOH electrolyte solutions. The specific capacitance values of the compounds were compared, and the results showed that trivalent boron (BCC_1) exhibited higher specific capacitance values than tetravalent boron (BCC_2) in both electrolyte solutions. In the presence of Na_2SO_4 electrolyte solution, the specific capacitance values of the trivalent (BCC_1) and tetravalent (BCC_2) boron compounds at a current density of 0.75 A/g were 135.21 and 94.87 F/g, respectively, while in the presence of KOH electrolyte, the specific capacitance values of the trivalent (BCC_1) and tetravalent (BCC_2) boron compounds at a current density of 0.75 A/g capacitance values were determined as 106.62 and 88.25 F/g, respectively. The cycling stability of the electrodes was also studied, and it was found that the capacitance of BCC_1 electrode increased gradually over the cycles, while the capacitance of BCC_2 electrode decreased. The study suggests that trivalent boron can be a promising material for supercapacitor applications. However, further research is required to optimize the cycling stability of the electrodes and understand the underlying mechanism.

Keywords: Supercapacitor; Boron-containing compounds (BCCs); Electrode; Characterization; Synthesis

1. Introduction

Rising population, industrialization, and widespread use of technology have resulted in considerable increases in energy consumption in emerging countries. As the world's energy demand grows, new energy resources must be produced, as well as existing energy resources must be stored for more efficient use. It is just as important to be able to store developed energy as it is to collect renewable energy [1–4]. Mechanical, chemical, and electrical systems are all viable options for storing energy [5–9]. Small-scale batteries and high-capacity capacitors have recently been the focus of the scientific investigation [10]. When compared to conventional capacitors, supercapacitors provide thousands of

* Corresponding author.

times more power and energy density, have shorter charging times, and have a longer lifespan [11,12]. In supercapacitors, the charge is held at the electrodes [13]. The supercapacitor's electrode is constructed of the most porous carbon-based materials. Supercapacitors made of metal oxide and conductive polymer have higher capacitance values than carbon-based supercapacitors [14–16].

Researchers have turned their attention to carbon-based electrodes due to factors such as the restricted conductivity of metal oxides, which have high capacitance properties, and the short cycle life of conductive polymers [17]. Carbon-based materials have grown in popularity as electrode materials in electrochemical devices due to their chemical durability and environmental responsibility, especially in acidic and basic environments and throughout a broad temperature range [18,19]. One of the major concerns with carbon-based materials used for electrodes is that the material agglomerates depending on the manufacturing process [20]. Moreover, many carbon-based electrodes [21,22] are impossible to make as a single layer, and the carbon-based sheets that are created have several chemical and topological defects. Using a lighter, more metallic material instead of carbon-based capacitors to increase specific capacitance beyond those capacitors is a novel approach. As a consequence, it is possible to identify boron-containing compounds [23].

In the previous two decades, the vast majority of boron-containing compounds have been synthesized and identified to have applications in a range of fields, including material and life sciences, medicine, energy, catalysis, and electronics [24–29]. Under the correct conditions, several structurally diverse trivalent and tetravalent boron-containing compounds may be easily synthesized in the laboratory. Because of the importance of boron-containing chemicals in a variety of industries, we started a research project to create boronate ester derivatives of them. Alkyl or aryl boronate ester derivatives as organocatalysts are arguably one of the biggest alternatives to their organic and metal counterparts in catalytic systems because of their incredible potential for cost savings, reductions in chemical waste and toxicity concerns, metal contamination, and drastic reaction conditions [30–33]. Boronate esters have grown more popular as a solution to the stability and chemoselectivity issues of homogeneous and heterogeneous catalysts due to their robust Lewis acidic properties, high stability, and low toxicity. Given the attractiveness of structurally diverse boron-containing compounds, alkyl and aryl boronate ester derivatives are bound to find increased utility in catalyst chemistry. In our previous studies [34–39], it was observed that boron-based electrodes increase the capacitance values as a result of experiments on supercapacitor applications of different boron-based materials. Parallel to these studies, in the presence of different electrolyte solutions (Na_2SO_4 and KOH), the trivalent and tetravalent boron-containing compounds ($C_{14}H_{14}BNO_2{\cdot}HCl$ (BCC_1) and $C_{38}H_{38}B_2Cl_2N_4O_4$ (BCC_2) synthesized in this work were used as electrodes in supercapacitor applications. The synthesized electrodes were named (BCC_1) and (BCC_2), respectively, the trivalent and tetravalent boron-containing compounds. According to all electrochemical investigations, the trivalent boron-containing (BCC_1) electrode material is a promising material for supercapacitor applications, with 135.21 F/g specific capacitance in Na_2SO_4 electrolyte.

2. Experimental section

2.1. Preparation of (BCC_1) and (BCC_2) electrodes

The synthesis of the trivalent (BCC_1) and tetravalent (BCC_2) boron compounds was carried out according to our previous study with a slight modification [24]. In summary, for the synthesis the trivalent (BCC_1) compound, a mixture of dopamine hydrochloride (1.0 g, 5.28 mmol) and phenylboronic acid (0.64 g, 5.28 mmol) in toluene (30 mL) was heated under reflux conditions with a Dean-Stark apparatus for 10 h. The reaction monitoring by TLC technique until observing a single well-defined peak. On completion of the reaction, the obtained solutions were cooled to room temperature, and followed by the excess toluene was evaporated. Then, the crude white crystal products were washed with n-hexane and purified by crystallization from toluene/hexane mixture affording pure trivalent (BCC_1) compound. Followed by, as a result of the reaction of the pure trivalent (BCC_1) (0.54 g, 1.96 mmol) and 4,4′-bipyridyl (0.15 g, 0.98 mmol) in $CHCl_3$ at a mole ratio of 2:1 under room conditions for 24 h, crystalline tetravalent (BCC_2) compound was obtained. The reaction route and structure schematic of the target trivalent (BCC_1) and tetravalent (BCC_2) boron compounds is shown in Fig. 1.

2.2. Preparation of electrode material for supercapacitor

0.05 g of trivalent (BCC_1) and tetravalent boron (BCC_2) compounds were added to the solvent polyvinylidene fluoride (PVDF, 0.02 g)+N-methyl-2-pyrrolidone (NMP) (1.0 mL). After complete mixing, 0.03 g of carbon nanotube (CNT) was added to the mixture. Then, 2.0 mL of NMP was added and mixed well. The resulting mixture was subjected to mixing in an ultrasonic water bath for 10 min. It was mixed on a magnetic stirrer for about 2 h. The resulting mixture is ready for spraying on nickel foam. The paper separator, the anode and cathode electrodes prepared by cutting in 15 mm circular diameters, and 6 M KOH as the electrolyte solution was placed in a sealed aluminum test apparatus to form the two-electrode cell configuration.

3. Results and discussion

The structural characteristics of trivalent (BCC_1) and tetravalent boron (BCC_2) compounds are investigated using X-ray diffraction (XRD, Rigaku SmartLab). The XRD diffraction patterns for (BCC_1) and (BCC_2) boron compounds are indicated in Fig. 2. In the region of $2\theta = 20°–60°$, XRD measurements are carried out. Both materials show a wide diffraction pattern in the region of $2\theta = 20°–30°$. Previous research has shown that both peaks belong to the (002) plane [40]. In XRD measurement, there are two key things to keep in mind. First and foremost, due to the wide diffraction peak produced for both samples, the full half-maximum width (FHMW) value of both samples is low. The low FHMW value might be used as a sign of the synthesized material's quality. The (002) plane occurs at various diffraction sites, according

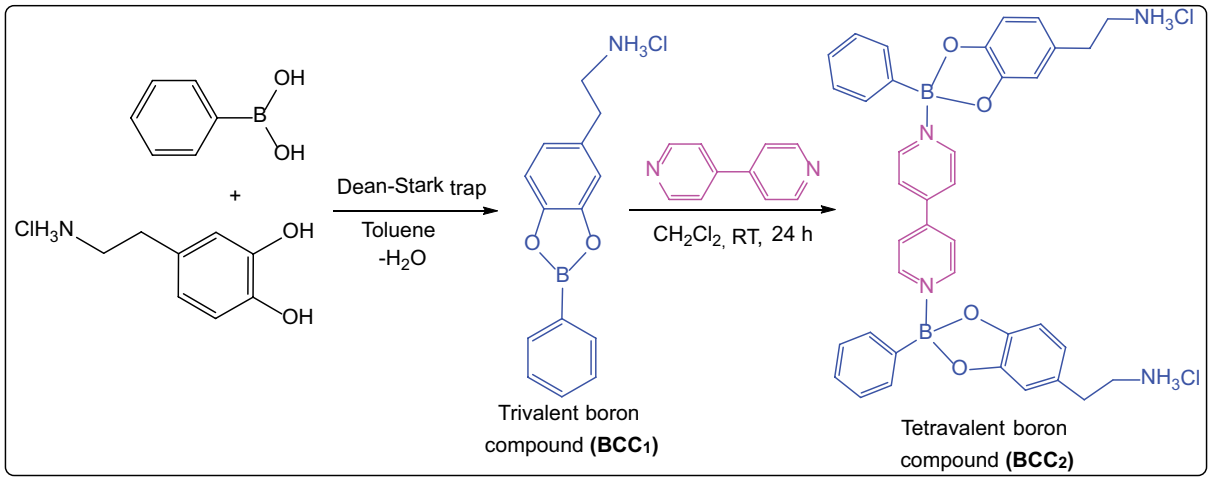

Fig. 1. Synthesis mechanism of the trivalent (BCC_1) and tetravalent boron (BCC_2) compounds.

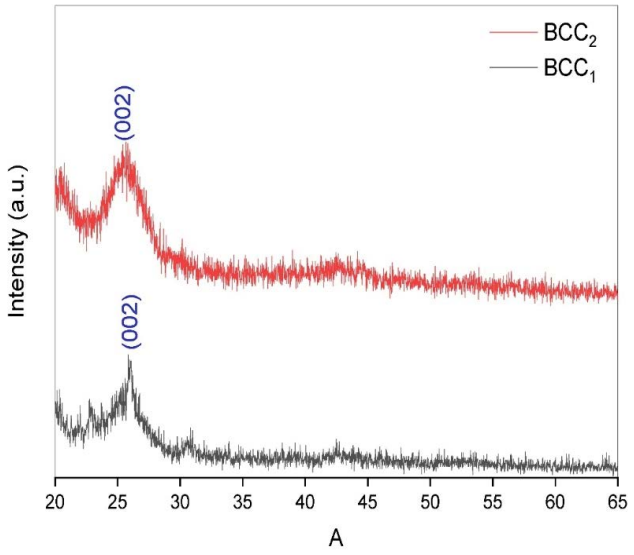

Fig. 2. X-ray diffraction patterns recorded for trivalent (BCC_1) and tetravalent boron (BCC_2) compounds.

to the second observation. The diffraction pattern for trivalent (BCC_1) boron compound, for example, is 2θ = 25.27°, but the identical peak occurs at 2θ = 25.65° for tetravalent boron (BCC_2) compound. The presence of a two boron (B) center in the structure of tetravalent boron (BCC_2) compound might be the cause of this condition.

Scanning electron microscopy (SEM, Zeiss Evo 55) is a method for elucidating the physical morphology of materials' surfaces. Fig. 3a shows the SEM image of trivalent (BCC_1) boron compound, while Fig. 3b demonstrates the SEM image of tetravalent boron (BCC_2) compound. Both images have a 30 μm scale and are recorded under 500X magnification. The main difference in the SEM images of (BCC_1) and (BCC_2) boron compounds is that trivalent (BCC_1) has a more porous structure compared to (BCC_2). This is seen when Brunauer–Emmett–Teller (BET, Micromeritics Instrument) surface areas of the samples are examined. While the BET surface area value for (BCC_1) is 117.27 m^2/g, this value decreases to 52.92 m^2/g for (BCC_1). It can be concluded that improving BET surface areas allows such materials to be used in electrochemical applications in a promising way.

Energy-dispersive X-ray (EDX, Quanta FEG 250) measurement is performed to elementally examine the trivalent (BCC_1) and tetravalent boron (BCC_2) compounds. The recorded EDX spectra for trivalent (BCC_1) and tetravalent boron (BCC_2) compounds are revealed in Fig. 3c and d, respectively. The atomic ratios (%) of the elements in the spectrum of trivalent (BCC_1) boron compound is 0.05 for B (K series), 13.81 for C (K series), 48.54 for N (K series), 0.05 for Cl (K series), and 37.52 for O (K series) while atomic ratios (%) of the elements in the spectrum of tetravalent boron (BCC_2) compound is 0.43 for B (K series), 1.76 for C (K series), 64.01 for N (K series), 1.01 for Cl (K series), and 32.79 for O (K series). It is observed in the EDX spectra the presence of chemical elements B, C, N, Cl, and O, suggesting clearly the success in the preparation of the trivalent (BCC_1) and tetravalent boron (BCC_2) compounds.

To examine the organic/inorganic components in trivalent (BCC_1) and tetravalent boron (BCC_2) compounds, Fourier-transform infrared spectroscopy (FTIR, IR-4000) measurements are performed. Fig. 4a and b reveal the FTIR spectra of trivalent (BCC_1) and tetravalent boron (BCC_2) compounds. When the FTIR spectra of trivalent (BCC_1) boron compound are examined, it is thought that the peaks observed at 3,086; 2,969–2,870; 1,616; 1,324; 1,115; 1,071; 814; 689 and 573 cm^{-1} are associated with Ar-CH, Aliph CH, C=C, B–O, C–O, B–C, C–H, C–O, and carbonyl group bonds, respectively. Similarly, it is determined that stretching-NH_2, Ar-CH, Aliph-CH, bending-NH_2, C=C, B–O, C–O, B–N, C–H, C–O, and carbonyl group bonds bonds for tetravalent boron (BCC_2) compound correspond to peaks observed at 3,340; 3,085; 2,981–2,854; 1,625 and 1,605; 1,495–1,451; 1,290; 1,120; 1,054; 805; 706 and 639 cm^{-1}, respectively.

In order to examine the capacitive behavior of the prepared electrode materials and the effect of the electrolyte liquid used on the supercapacitors, four different supercapacitor cells with two electrode configurations are established. The resistance, capacitance, and stability of the prepared supercapacitors are tested using electrochemical

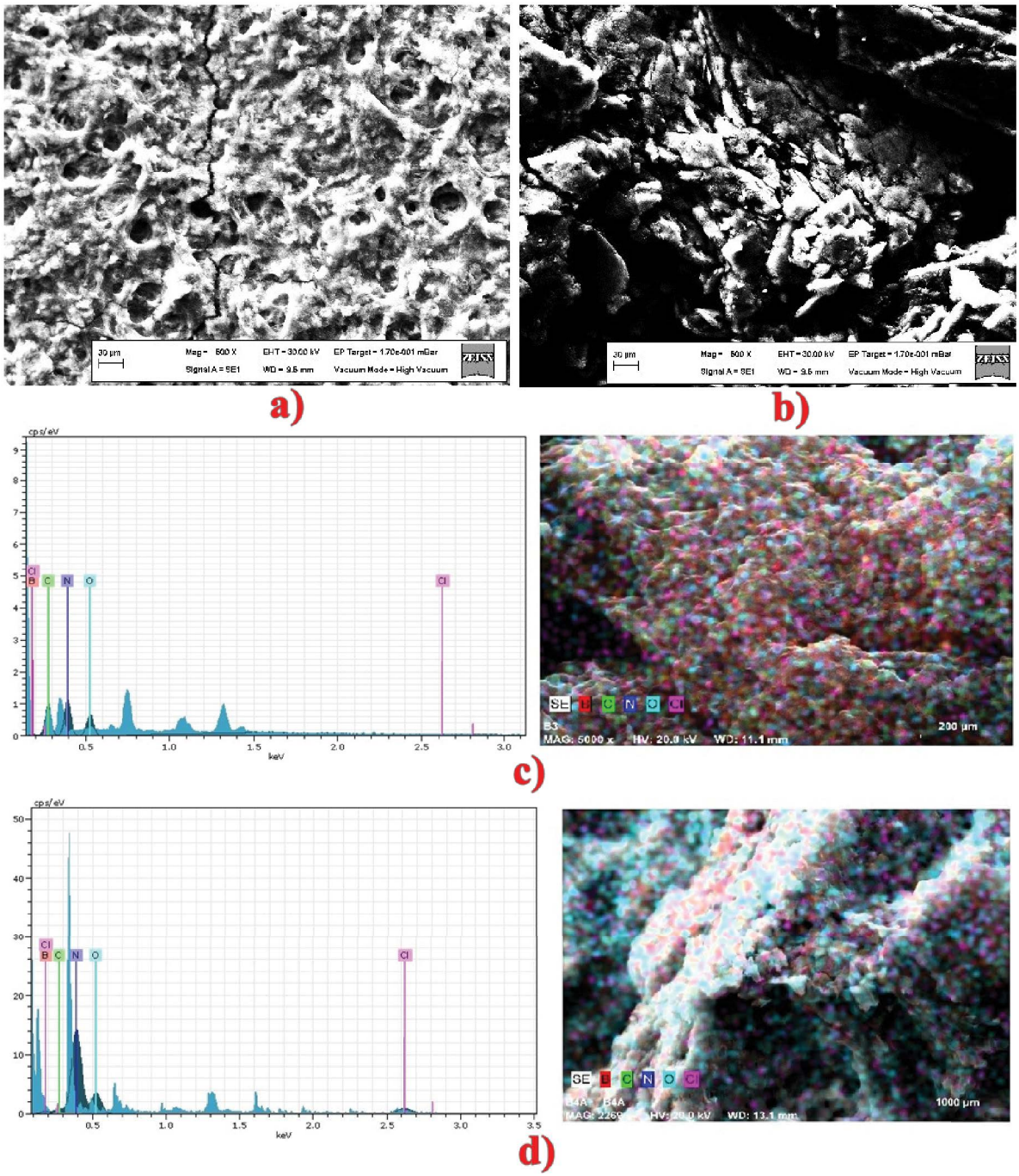

Fig. 3. Recorded scanning electron microscopy image for (a) (BCC_1), (b) (BCC_2) boron compounds and the energy-dispersive X-ray spectrum of (c) trivalent (BCC_1), (d) tetravalent (BCC_2) boron compounds.

characterization techniques. Fig. 5 presents the characteristic curves of the capacitor at different scanning speeds (in the range of –0.8–0.0 V) using the cyclic voltammetry (CV) technique for all materials. Although all materials' CV curves are similar to the ideal supercapacitor curves, redox fluctuations are observed in the CV curves of tetravalent boron (BCC_2) material, which are not very obvious. Since the access of ions into the pores of the active material is reduced at high scanning speed, CV curves diverge from ideal curves at high scanning rates.

Charge-discharge curves of the supercapacitor are obtained using the galvanostatic charge discharge (GCD) technique and are given in Fig. 6. At high current densities, the charge-discharge curves overly resemble the isosceles triangle structure, which is the ideal supercapacitor curve. The perfection of the curves shows that the ion exchange

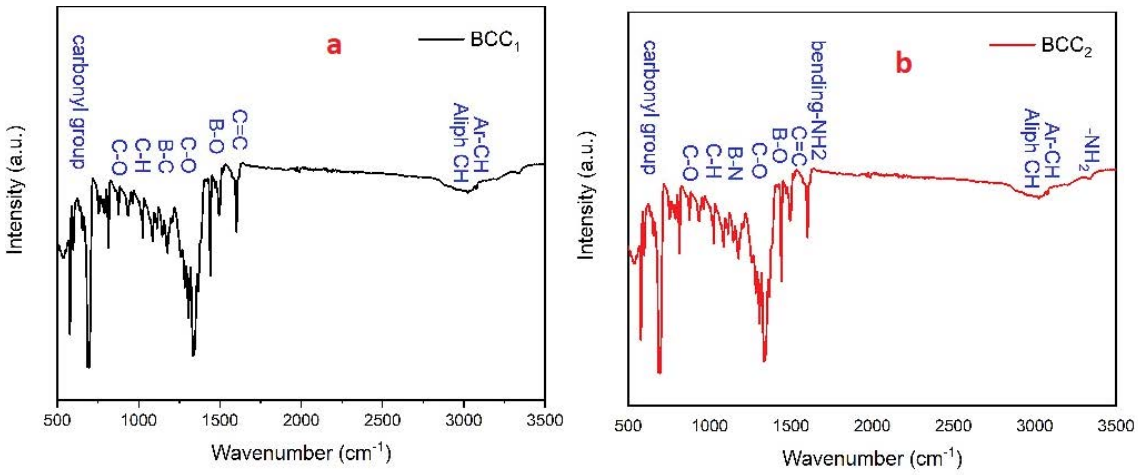

Fig. 4. Fourier-transform infrared spectra recorded for (a) trivalent (BCC_1) and (b) tetravalent boron (BCC_2) compounds.

between the electrode surfaces and the electrolyte liquid occurs rapidly and reversibly. At low current densities, the curves diverge from ideal curves. The reason for the divergence of the curves during discharge is thought to be the epoxy conduction effect of boron and this shows the capacitive behavior of the supercapacitor device [41]. The specific capacitance of the electrodes was calculated by Eq. (1) using charge-discharge curves:

$$C = \frac{\left(2 \cdot I \cdot \Delta t\right)}{\left(m \cdot \Delta V\right)}$$

where m(g) given in the equation is the amount of active material on an electrode; Δt(s) is the discharge time; I(A), current; ΔV(V) denotes the applied voltage range. The capacitance values of the electrodes at different current densities and the FTIR drops on the electrodes are given in Table 1. While the trivalent (BCC_1) boron material exhibited better capacitance values at low current densities, the supercapacitor cell formed with the Na_2SO_4 electrolytes and tetravalent (BCC_2) boron material exhibited better capacitance values at current densities above 1 A/g. At high current densities, the materials showed much higher capacitance values in the Na_2SO_4 electrolyte than in KOH. This shows that the materials have better electron exchange with the Na_2SO_4 electrolyte due to their geometric structure. The voltage drops on the electrodes prepared using trivalent (BCC_1) boron material are much higher than tetravalent (BCC_2) boron material. The voltage drops in supercapacitor cells prepared using Na_2SO_4 electrolyte are lower than that of KOH. As a matter of fact, the Nyquist curves given in Fig. 6a also support these results. At the 0.75 A/g current density, 4.22 Wh/cm^2 energy density at 303.66 Wk/cm^2 power density, 3.92 Wh/cm^2 energy density at 307.52 Wk/cm^2 power density, 6.01 Wh/cm^2 energy density at 308.90 Wk/cm^2 power density and 4.74 Wh/cm^2 energy density at 312.98 Wk/cm^2 power density is obtained for (BCC_2)-Na_2SO_4, (BCC_2)-KOH, (BCC_1)-Na_2SO_4, (BCC_1)-KOH supercapacitors, respectively. The highest energy density was obtained for (BCC_1)-Na_2SO_4 material and it is more suitable for applications requiring high energy density compared to other materials.

Nyquist curves of supercapacitor cells obtained as a result of electrochemical impedance spectroscopy (EIS) technique are given in Fig. 7a. Measurements are taken between 1.0 and 100 kHz with an amplitude of 10 mV. Equivalent series resistances (R_S) of supercapacitor cells in the high frequency region of Nyquist curves are obtained as 1.75, 1.00, 2.87 and 1.13 Ω for (BCC_2)-Na_2SO_4, (BCC_2)-KOH, (BCC_1)-Na_2SO_4, and (BCC_1)-KOH, respectively. The R_S resistances of the cells established with KOH electrolyte are lower. The low resistance value supports the low voltage drops caused by the electrodes and therefore the power transfers can be made at high levels [42,43]. The diameter of the semicircle expressing the interfacial charge transfer resistance (R_{ct}) at medium frequencies is obtained as 4.27, 8.48, 8.98, and 12.54 Ω for (BCC_2)-Na_2SO_4, (BCC_2)-KOH, (BCC_1)-Na_2SO_4, and (BCC_1)-KOH, respectively. The R_{ct} resistance of the (BCC_1) supercapacitors is higher than the resistance of the (BCC_2) supercapacitors, and the R_{ct} resistance of the materials in the KOH solution is higher. This shows that oxidation reactions take place in the KOH electrolyte liquid. At low frequencies, the slope of the Nyquist curves obtained close to the ideal supercapacitor slope (90°) and these values are approximately 79.82°, 82.39°, 76.08° and 82.55° for (BCC_2)-Na_2SO_4, (BCC_2)-KOH, (BCC_1)-Na_2SO_4, and (BCC_1)-KOH, respectively. These results show that there is a perfect interaction between the electrode main materials and the electrolyte, the diffusion path of the ions in the electrolyte is short and the diffusion resistance is very low [44–46]. Especially, the ionic conductivity and the small ion radius of KOH ensured easy access of KOH ions to the pores of the electrode material [47].

In order to test the stability of the four different supercapacitors, the cells are subjected to long charge-discharge cycles and the results are given in Fig. 7b. For the (BCC_2)-Na_2SO_4 cell, the capacitance value of the electrodes increases considerably and starts to decrease again after 95 cycles. After 100 cycles, there is still an increase of 182.37% compared to the initial capacitance value. Similarly, in the (BCC_2)-Na_2SO_4 cell, the capacitance value of the electrodes increases until the first 60 cycles, then starts to decrease, and after 100 cycles, there is still a 41.31% increase in capacitance compared to the first value. This increase may be due to the

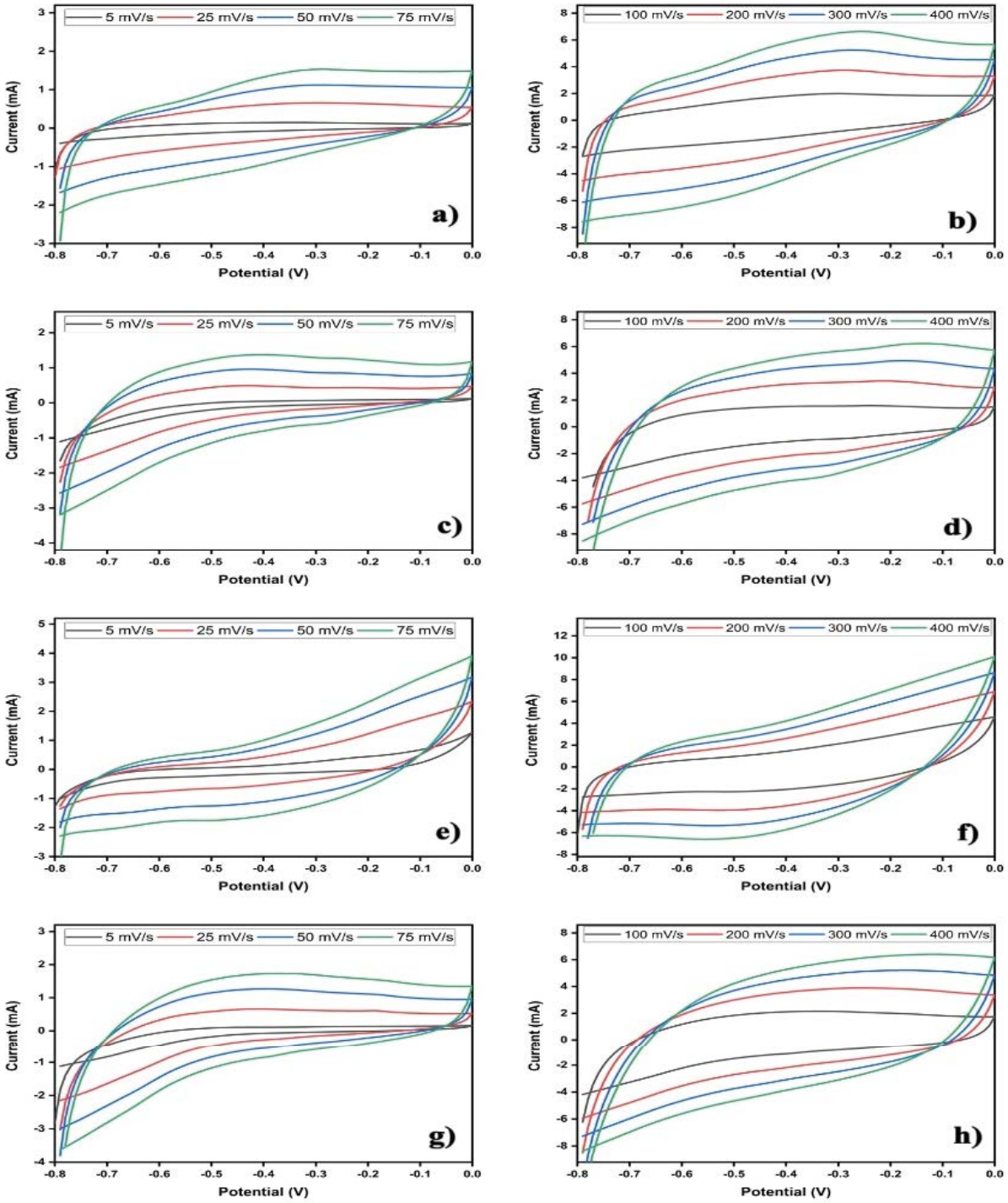

Fig. 5. Cyclic voltammetry curves of (BCC_2)-Na_2SO_4, (BCC_2)-KOH, (BCC_1)-Na_2SO_4, and (BCC_1)-KOH supercapacitor cells at different scanning rates.

gradual activation of the surface and thus the better access of electrolyte ions to the pores of the (BCC_2) electrode material with progressive cycles [48]. Contrary to these electrodes, the capacitance values of (BCC_2)-KOH, and (BCC_1)-KOH electrodes decrease by 64.54% and 28.41%, respectively.

Active materials used in electrode preparation are the most basic components that determine the capacitance values and energy densities of the supercapacitors to be used in the application. The type of electrode used, preparation method and doped chemical compounds are important factors affecting the electrochemical properties of the supercapacitor [49]. In the literature, in the studies of boron supercapacitors, supercapacitors have been produced by doping boron to the activated carbons. In the study of boron doped graphene

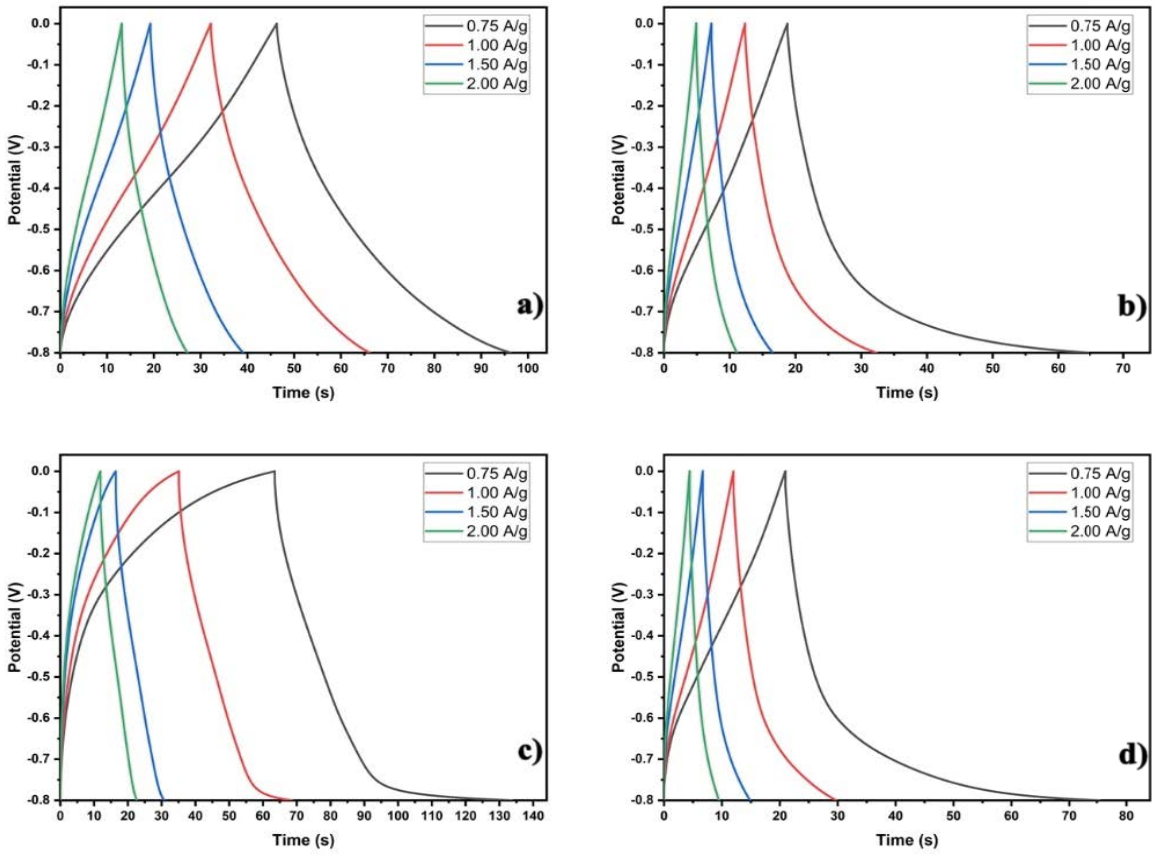

Fig. 6. Charge-discharge curves of (BCC_2)-Na_2SO_4, (BCC_2)-KOH, (BCC_1)-Na_2SO_4, and (BCC_1)-KOH supercapacitor cells at different current densities.

Table 1
Capacitance values of electrodes at different current densities and voltage drops on the electrodes

Current density	(BCC_2)-Na_2SO_4		(BCC_2)-KOH		(BCC_1)-Na_2SO_4		(BCC_1)-KOH	
	Capacitance (F/g)	Infrared drop (mV)	Capacitance (F/g)	Infrared drop (mV)	Capacitance (F/g)	Infrared drop (mV)	Capacitance (F/g)	Infrared drop (mV)
0.75 A/g	94.87	9	88.25	20	135.21	23	106.62	33
1.0 A/g	86.19	12	51.75	27	86.70	30	46.93	46
1.5 A/g	76.05	17	37.00	42	58.02	44	33.48	67
2.0 A/g	72.28	23	33.04	53	57.14	57	28.44	87

nanosheets prepared through hydrothermal using boric acid for electrode application, the electrode exhibited a maximum specific capacitance of 113 F/g at 1 A/g. The supercapacitor could deliver energy density in the range of 5.96–4.64 Wh/kg and power density in the range of 0.16–0.97 kW/kg [50]. In another study, boron and nitrogen co-doped porous carbons were prepared for supercapacitor electrodes and samples showed the specific capacitance up to 268 and 173 F/g, with the current of 0.1 A/g. At the current density of 1 A/g, the energy densities were 3.8 and 3.0 Wh/g and the power densities were 165 and 201 Wk/g [51]. When nitrogen and boron co-doped densified laser-induced graphene was used for supercapacitor electrode, the specific areal capacitance was obtained 40.4 mF/cm^2 at 0.05 mA/cm^2 and capacitor showed areal energy density of 5.61 μ/Wh·cm^2 at a power density of 0.025 mW·cm^2 [52]. Boron carbon nitride electrodes fabricated via laser patterning technique, device showed specific capacitance 17 mF·cm^2 at current density of 1 mA·cm^2 [53]. Boron-doped diamond electrode possesses 15.7 Ω·cm^2 R_S value, a maximum specific capacitance of 6.44 mF·cm^2 at a current density of 0.10 mA·cm^2 in another study [54]. The capacities, energy and power densities of four different supercapacitors prepared in this study, which is carried out considering the base material used, the doped chemical compounds, the preparation method and the type of electrode used, are very close to the results given in the literature.

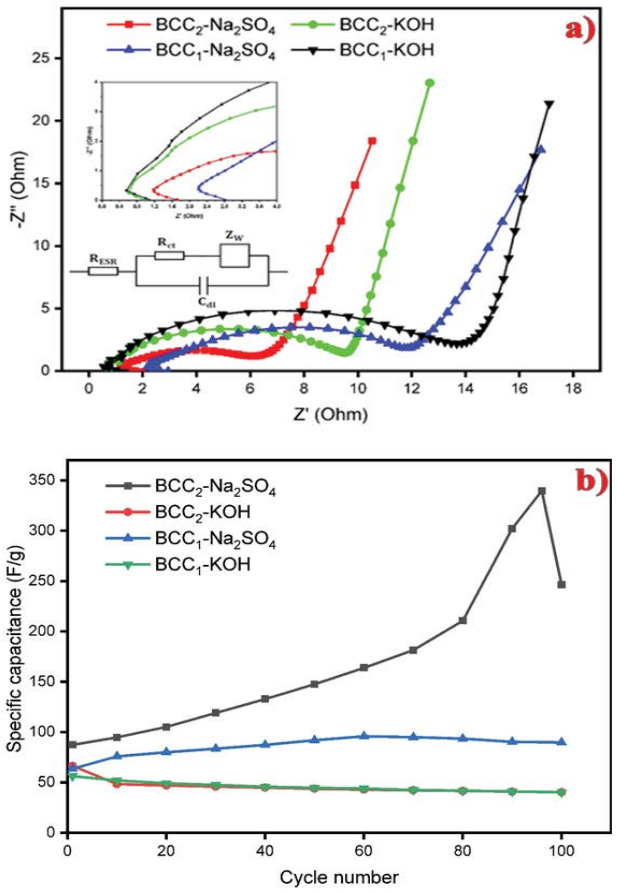

Fig. 7. (a) Impedance curves and (b) cyclic performance of (BCC_2)-Na_2SO_4, (BCC_2)-KOH, (BCC_1)-Na_2SO_4, (BCC_1)-Na_2SO_4-KOH electrodes.

Therefore, considering the electrochemical results of the electrodes, it is thought that the produced supercapacitors will occupy an important place in the field of energy storage.

4. Conclusion

In the present study, the synthesized $C_{14}H_{14}BNO_2$·HCl (BCC_1) and $C_{38}H_{38}B_2Cl_2N_4O_4$ (BCC_2) were used as electrodes in supercapacitor applications in the presence of different electrolyte solutions (Na_2SO_4 and KOH). In the presence of Na_2SO_4 electrolyte solution, the specific capacitance values of the trivalent (BCC_1) and tetravalent (BCC_2) boron compounds at a current density of 0.75 A/g were 135.21 and 94.87 F/g, respectively, while in the presence of KOH electrolyte, the specific capacitance values of the trivalent (BCC_1) and tetravalent (BCC_2) boron compounds at a current density of 0.75 A/g capacitance values were determined as 106.62 and 88.25 F/g, respectively. It was clearly shown experimentally that trivalent boron (BCC_1) compound was more active than tetravalent boron (BCC_2) compound in the presence of both different electrolyte solutions. Moreover, for the (BCC_2)-Na_2SO_4 cell, the capacitance value of the electrodes increased considerably and started to decrease again after 95 cycles. After 100 cycles, there was still an increase of 182.37% compared to the initial capacitance value. Similarly, in the (BCC_1)-Na_2SO_4 cell, the capacitance value of the electrodes increased until the first 60 cycles, then started to decrease, and after 100 cycles, there was still a 41.31% increase in capacitance compared to the first value. This increase might be due to the gradual activation of the surface and thus the better access of electrolyte ions to the pores of the (BCC_1) electrode material with progressive cycle. Contrary to these electrodes, the capacitance values of (BCC_2)-KOH, and (BCC_1)-KOH electrodes decreased by 64.54% and 28.41%, respectively. As a result, trivalent boron (BCC_1) compound, one of the boron-containing compounds, can be used as a promising material in super capacitor applications.

Data availability

Not applicable

Ethical approval

The authors declare that they have no conflict of interest.

Consent to participate

Not applicable

Consent to publish

Not applicable

Competing interests

The authors declare that they have no competing interests.

References

[1] H. An, A. Razzaq, M. Haseeb, L.W.W. Mihardjo, The role of technology innovation and people's connectivity in testing environmental Kuznets curve and pollution heaven hypotheses across the Belt and Road host countries: new evidence from Method of Moments Quantile Regression, Environ. Sci. Pollut. Res., 28 (2021) 5254–5270.
[2] O. Ellabban, H. Abu-Rub, F. Blaabjerg, Renewable energy resources: current status, future prospects and their enabling technology, Renewable Sustainable Energy Rev., 39 (2014) 748–764.
[3] C. Scheel, E. Aguiñaga, B. Bello, Decoupling economic development from the consumption of finite resources using circular economy. A model for developing countries, Sustainability, 12 (2020) 1291–1312.
[4] R. Sharma, A. Sinha, P. Kautish, Does renewable energy consumption reduce ecological footprint? Evidence from eight developing countries of Asia, J. Cleaner Prod., 285 (2021) 124867, doi: 10.1016/j.jclepro.2020.124867.
[5] S. Zhang, X. Xu, T. Lin, P. He, Recent advances in nanomaterials for packaging of electronic devices, J. Mater. Sci. - Mater. Electron., 30 (2019) 13855–13868.
[6] Y. Bai, C. Liu, T. Chen, W. Li, S. Zheng, Y. Pi, Y. Luo, H. Pang, MXene-copper/cobalt hybrids via Lewis acidic molten salts etching for high performance symmetric supercapacitors, Angew. Chem., 133 (2021) 25522–25526.
[7] Q. Jing, W. Li, J. Wang, X. Chen, H. Pang, Calcination activation of three-dimensional cobalt organic phosphate nanoflake assemblies for supercapacitors, Inorg. Chem. Front., 8 (2021) 4222–4229.
[8] C. Liu, Y. Bai, W. Li, F. Yang, G. Zhang, H. Pang, *In-situ* growth of three-dimensional MXene/metal–organic framework

composites for high-performance supercapacitors, Angew. Chem., 134 (2022) e202116282, doi: 10.1002/anie.202116282.
[9] H. Zhou, S. Zheng, X. Guo, Y. Gao, H. Li, H. Pang, Ordered porous and uniform electric-field-strength micro-supercapacitors by 3D printing based on liquid-crystal V_2O_5 nanowires compositing carbon nanomaterials, J. Colloid Interface Sci., 628 (2022) 24–32.
[10] Y. Xiu, L. Cheng, L. Chunyan, Research on hybrid energy storage system of super-capacitor and battery optimal allocation, J. Int. Counc. Electr. Eng., 4 (2014) 341–347.
[11] M. Horn, J. MacLeod, M. Liu, J. Webb, N. Motta, Supercapacitors: a new source of power for electric cars?, Econ. Anal. Policy., 61 (2019) 93–103.
[12] H. Xu, M. Shen, The control of lithium-ion batteries and supercapacitors in hybrid energy storage systems for electric vehicles: a review, Int. J. Energy Res., 45 (2021) 20524–20544.
[13] S. Özarslan, M.R. Atelge, H.D. Kıvrak, S. Horoz, C. Yavuz, M. Kaya, S. Ünalan, A double-functional carbon material as a supercapacitor electrode and hydrogen production: Cu-doped tea factory waste catalyst, J. Mater. Sci. - Mater. Electron., 32 (2021) 28909–28918.
[14] D. Nandi, V.B. Mohan, A.K. Bhowmick, D. Bhattacharyya, Metal/metal oxide decorated graphene synthesis and application as supercapacitor: a review, J. Mater. Sci., 55 (2020) 6375–6400.
[15] S. Özarslan, M.R. Atelge, M. Kaya, S. Ünalan, Production of dual functional carbon material from biomass treated with NaOH for supercapacitor and catalyst, Energy Storage, 3 (2021) e257, doi: 10.1002/est2.257.
[16] P. Veerakumar, A. Sangili, S. Manavalan, P. Thanasekaran, K.-C. Lin, Research progress on porous carbon supported metal/metal oxide nanomaterials for supercapacitor electrode applications, Ind. Eng. Chem. Res., 59 (2020) 6347–6374.
[17] Z.S. Iro, C. Subramani, S. Dash, A brief review on electrode materials for supercapacitor, Int. J. Electrochem. Sci., 11 (2016) 10628–10643.
[18] R.S. Kate, S.A. Khalate, R.J. Deokate, Overview of nanostructured metal oxides and pure nickel oxide (NiO) electrodes for supercapacitors: a review, J. Alloys Compd., 734 (2018) 89–111.
[19] P. Simon, Y. Gogotsi, Perspectives for electrochemical capacitors and related devices, Nat. Mater., 19 (2020) 1151–1163.
[20] S. Nayak, A. Soam, J. Nanda, C. Mahender, M. Singh, D. Mohapatra, R. Kumar, Sol–gel synthesized $BiFeO_3$–graphene nanocomposite as efficient electrode for supercapacitor application, J. Mater. Sci. - Mater. Electron., 29 (2018) 9361–9368.
[21] M. Akdemir, D.E. Karakaş, M. Kaya, Synthesis of a dual-functionalized carbon-based material as catalyst and supercapacitor for efficient hydrogen production and energy storage: Pd-supported pomegranate peel, Energy Storage, 4 (2022) e284, doi: 10.1002/est2.284.
[22] I.I.G. Inal, M. Akdemir, M. Kaya, *Microcystis aeruginosa* supported-Mn catalyst as a new promising supercapacitor electrode: a dual functional material, Int. J. Hydrogen Energy, 46 (2021) 21534–21541.
[23] C. Zhan, P. Zhang, S. Dai, D. Jiang, Boron supercapacitors, ACS Energy Lett., 1 (2016) 1241–1246.
[24] A. Kilic, E. Aytar, L. Beyazsakal, A novel dopamine-based boronate esters with the organic base as highly efficient, stable, and green catalysts for the conversion of CO_2 with epoxides to cyclic carbonates, Energy Technol., 9 (2021) 2100478, doi: 10.1002/ente.202100478.
[25] A. Kilic, İ.H. Kaya, I. Ozaslan, M. Aydemir, F. Durap, Catechol-type ligand containing new modular design dioxaborinane compounds: use in the transfer hydrogenation of various ketones, Catal. Commun., 111 (2018) 42–46.
[26] A. Kilic, İ.H. Kaya, I. Ozaslan, M. Aydemir, F. Durap, Synthesis and effective catalytic performance in cycloaddition reactions with CO_2 of boronate esters versus N-heterocyclic carbene (NHC)-stabilized boronate esters, Sustainable Energy Fuels, 4 (2020) 5682–5696.
[27] Q. Meng, M. Wang, M. Vicente, Tetravalent Boron-Based, M.M. Pereira, M.J.F. Calvete, Eds., Sustainable Synthesis of Pharmaceuticals: Using Transition Metal Complexes as Catalysts, De Gruyter, 2018, p. 253.
[28] M. Richold, Boron exposure from consumer products, Biol. Trace Elem. Res., 66 (1998) 121–129.
[29] M.M. Smedskjaer, J.C. Mauro, R.E. Youngman, C.L. Hogue, M. Potuzak, Y. Yue, Topological principles of borosilicate glass chemistry, J. Phys. Chem. B, 115 (2011) 12930–12946.
[30] A. Chardon, J. Rouden, J. Blanchet, Borinic acid mediated hydrosilylations: reductions of carbonyl derivatives, Eur. J. Org. Chem., 2019 (2019) 995–998.
[31] P. Eisenberger, C. Crudden, Borocation catalysis, Dalton Trans., 46 (2017) 4874–4887.
[32] A. Kilic, M. Durgun, F. Durap, M. Aydemir, The chiral boronate-catalyzed asymmetric transfer hydrogenation of various aromatic ketones to high-value alcohols: preparation and spectroscopic studies, J. Org. Chem., 890 (2019) 1–12.
[33] T. Mahdi, D.W. Stephan, Facile protocol for catalytic frustrated Lewis pair hydrogenation and reductive deoxygenation of ketones and aldehydes, Angew. Chem. Int. Ed., 54 (2015) 8511–8514.
[34] M. Akdemir, T.A. Hansu, A. Kilic, L. Beyazsakal, M. Kaya, Sabit Horoz, Investigation of electrochemical properties of tri-and tetravalent boronate ester compounds for supercapacitor applications, Ionics, 28 (2022) 5199–5210.
[35] T.A. Hansu, A. Kilic, R. Soylemez, M. Akdemir, M. Kaya, S. Horoz, The preparation and characterization of the novel mono-/binuclear boron-based materials for supercapacitor electrode applications, Chem. Pap., 76 (2022) 7111–7122.
[36] G. Chen, Z. Hu, H. Su, J. Zhang, D. Wang, Ultrahigh level heteroatoms doped carbon nanosheets as cathode materials for Zn-ion hybrid capacitor: the indispensable roles of B containing functional groups, Colloids Surf., A, 656 (2023) 130528, doi: 10.1016/j.colsurfa.2022.130528.
[37] Z. Sun, X. Han, and D.J.J.o.E.S. Wang, Zinc-iodine battery-capacitor hybrid device with excellent electrochemical performance enabled by a robust iodine host, J. Energy Storage, 62 (2023) 106857, doi: 10.1016/j.est.2023.106857.
[38] D. Wang, Z. Zhang, J. Sun, Z. Lu, From volatile ethanolamine to highly N, B dual doped carbon superstructures for advanced Zn-ion hybrid capacitors: unveiling the respective effects heteroatom functionalities, J. Electrochem. Soc., 169 (2022) 070511, doi: 10.1149/1945-7111/ac7e71.
[39] S. Wang, Z. Hu, Z. Pan, D. Wang, Mohr's salt assisted KOH activation strategy to customize S-doped hierarchical carbon frameworks enabling satisfactory rate performance of supercapacitors, J. Alloys Compd., 876 (2021) 160203, doi: 10.1016/j.jallcom.2021.160203.
[40] Y. Guo, C. Yan, P. Wang, L. Rao, C. Wang, Doping of carbon into boron nitride to get the increased adsorption ability for tetracycline from water by changing the pH of solution, Chem. Eng. J., 387 (2020) 124136, doi: 10.1016/j.cej.2020.124136.
[41] L. Manjakkal, C.G. Núñez, W. Dang, R. Dahiya, Flexible self-charging supercapacitor based on graphene-Ag-3D graphene foam electrodes, Nano Energy, 51 (2018) 604–612.
[42] Q. Cheng, J. Tang, J. Ma, H. Zhang, N. Shinya, L.C. Qin, Graphene and nanostructured MnO_2 composite electrodes for supercapacitors, Carbon, 49 (2011) 2917–2925.
[43] X. Yan, Y. Yu, X. Yang, Effects of electrolytes on the capacitive behavior of nitrogen/phosphorus co-doped nonporous carbon nanofibers: an insight into the role of phosphorus groups, RSC Adv., 4 (2014) 24986–24990.
[44] J. Gamby, P.L. Taberna, P. Simon, J.F. Fauvarque, M. Chesneau, Studies and characterisations of various activated carbons used for carbon/carbon supercapacitors, J. Power Sources, 101 (2001) 109–116.
[45] X. Zhu, S. Yu, K. Xu, Y. Zhang, L. Zhang, G. Lou, Y. Wu, E. Zhu, H. Chen, Z. Shen, B. Bao, S. Fu, Sustainable activated carbons from dead ginkgo leaves for supercapacitor electrode active materials, Chem. Eng. Sci., 181 (2018) 36–45.
[46] S. Ghosh, T. Mathews, B. Gupta, A. Das, N. Gopala Krishna, M. Kamruddin, Supercapacitive vertical graphene nanosheets in aqueous electrolytes, Nano-Struct. Nano-Objects, 10 (2017) 42–50.
[47] X. Zhang, X. Wang, L. Jiang, H. Wu, C. Wu, J. Su, Effect of aqueous electrolytes on the electrochemical behaviors of

supercapacitors based on hierarchically porous carbons, J. Power Sources, 216 (2012) 290–296.
[48] C. Zequine, C.K. Ranaweera, Z. Wang, S. Singh, P. Tripathi, O.N. Srivastava, B.K. Gupta, K. Ramasamy, P.K. Kahol, P.R. Dvornic, R.K. Gupta, High performance and flexible supercapacitors based on carbonized bamboo fibers for wide temperature applications, Sci. Rep., 6 (2016) 1–10.
[49] I.I.G. Inal, M. Akdemir, M. Kaya, *Microcystis aeruginosa* supported-Mn catalyst as a new promising supercapacitor electrode: a dual functional material, Int. J. Hydrogen Energy, 46 (2021) 21534–21541.
[50] V. Thirumal, A. Pandurangan, R. Jayavel, R. Ilangovan, Synthesis and characterization of boron doped graphene nanosheets for supercapacitor applications, Synth. Met., 220 (2016) 524–532.
[51] H. Guo, Q. Gao, Boron and nitrogen co-doped porous carbon and its enhanced properties as supercapacitor, J. Power Sources, 186 (2009) 551–556.
[52] M. Khandelwal, C.V. Tran, J. Lee, J.B. In, Nitrogen and boron co-doped densified laser-induced graphene for supercapacitor applications, Chem. Eng. J., 428 (2022) 131119, doi: 10.1016/j.cej.2021.131119.
[53] I. Karbhal, A. Basu, A. Patrike, M.V. Shelke, Laser patterning of boron carbon nitride electrodes for flexible micro-supercapacitor with remarkable electrochemical stability/capacity, Carbon, 171 (2021) 750–757.
[54] J. Zhang, X. Yu, Z.Q. Zhang, Z.Y. Zhao, Preparation of boron-doped diamond foam film for supercapacitor applications, Appl. Surf. Sci., 506 (2020) 144645, doi: 10.1016/j.apsusc.2019.144645.